VTT Technical Research Centre of Finland

The Performance and Force Coefficients of Flapping Foil

Martio, Jussi; Sánchez-Caja, Antonio

Published in:
Proceedings 31st Symposium Naval Hydrodynamics

Published: 01/01/2016

Document Version
Publisher's final version

31st Symposium on Naval Hydrodynamics
Monterey, California, 11-16 September 2016

The Performance and Force Coefficients of Flapping Foil

J. Martio, A. Sánchez-Caja
(VTT-Technical Research Center of Finland)

ABSTRACT

The added mass and damping coefficients of a flapping foil propulsor are investigated using an URANS method with the k-omega turbulence model for two Reynolds numbers. First, computed performance coefficients are compared with experimental results from the open literature. Even though the flow regime is not exactly the same, reasonably good agreement was found between the current and published results. Then, the foil forces are evaluated in terms of added mass and damping coefficients. The viscous added mass and damping components are determined using an approximate first order harmonic fitting. The coefficients were parametrized using theoretical angle of attack and Strouhal number. They were determined in two coordinate systems, i.e. in the inertial and body-fixed coordinate ones. The choice of coordinate system does not have considerable influence in the parametrization of the added mass coefficient. However, the contours of constant damping coefficient were slightly different in the parametric space. A particular case is analyzed in more detail for two Reynolds numbers. Flow features like separation are shown how to affect added mass coefficients. The separated flow seems to reduce the performance of the foil.

INTRODUCTION

Propulsion systems of high efficiency have been investigated quite intensively during the last two decades. One example is the use of oscillating foils as a propulsion concept alternative to the traditional marine propeller. From a hydrodynamic standpoint, the concept has a potential for increasing the propulsive efficiency if adequate mechanisms are used.

Experimental work concerning the oscillating foils was published in Anderson et al. (1998). The NACA 0012 foil was tested at a Reynolds number around 40000. The optimum foil performance was found in the range of Strouhal numbers of 0.2-0.4 and angles of attack between 20-30 deg. Read et al. (2003) recorded planform-area-based thrust coefficients of 2.4 for 35-deg maximum angle of attack and efficiencies of up to 71.5% for 15-deg maximum angle of attack. A plateau of good efficiency, in the range of 50–60% was observed. However, efficiencies were not as large as those reported in the previous paper. Hover et al. (2004) found that the best efficiency was to be found with the least content of high harmonics in the angle of attack, i.e. with pure sinusoidal shape, the reason of which was attributed to the production of a “pure” reverse Karman street in the wake.

The oscillating foils have been studied also extensively by theoretical methods. The influence of kinematic parameters, like flapping frequency, amplitude and phase difference between pure plunge and pitch motion on the thrust generation and propulsive efficiency has been studied extensively, for example, Isogai et al. (1999) and Young and Lai (2004). Parameters related to foil geometric have also been investigated, for example, Cebeci et al. (2004) who found a negligible effect of increasing thickness on the propulsive efficiency of a plunging airfoil or Ashraf (2010) who studied numerically using RANS and panel codes the effect of thickness and camber for Reynolds number ranging 200-2,000,000. Barannyk et al. (2012) investigated the influence of foil flexibility in thrust production.

Vermeiden et al. (2012) conducted model tests for flapping propulsors of a container ship. The efficiency variations were measured at a higher Reynolds number (200,000) by varying systematically loading, pitching amplitude, chord-

length, chordwise flexibility and fin-spacing. They found systematically that the most efficient estimated maximum angle of attack is 10 to 11 degrees in the range of parameters where they performed the measurements. An unexpected result of the tests was the strong decrease of efficiency with growing chord–heave ratios, which cannot be explained by considerations on aspect ratio, reduced frequency or viscous losses.

Recently, Sanchez-Caja and Martio (2016) illustrated the impact of added mass terms on the performance of flapping foils. The influence of such terms on efficiency was not paid much attention in the previous literature. The unexpected reductions of efficiency when doubling the chord length for a constant thrust condition are shown to be a consequence of added mass terms both for oscillating foils and foil wheels. The paper suggests that understanding added-mass effects is essential for flapping foil optimization.

In this paper, URANS simulations on a flapping foil are compared with published experimental results. First, the global performance of the propulsion device is evaluated by URANS method for two Reynolds numbers. Then the added mass and damping coefficients are determined by applying a harmonic fitting to the total force. This analysis is carried out for the vertical force using two coordinate systems, an inertial and a body-fixed reference systems.

NUMERICAL METHOD

The flow simulation in FINFLO is based on the solution of the RANS equations by a finite volume method using the pressure correction method.

The spatial discretization is carried out by a finite volume method. Second- and third-order upwind-biased (MUSCL) schemes are used for the discretization of the convection terms and a second-order central-difference scheme is utilized for the diffusion. The pressure gradient is centrally differenced and a Rhie-Chow type dissipation is applied. A multigrid method is used for the acceleration of convergence. Solutions on coarse grid levels are used as a starting point for the calculation in order to accelerate convergence. A detailed description of the numerical method including discretization of the governing equations, solution algorithm, boundary conditions, etc. are described by Sánchez-Caja et al. (2006) and by Miettinen and Siikonen (2015). Several turbulence models are implemented in FINFLO. In these calculations the k-omega turbulence model is used. Time-accurate calculations are started by using a quasi-steady solution as an initial guess. In the time-accurate calculations part of the grid is rotating and part of the grid is stationary. The sliding mesh technique is used to treat the interface between the rotating and the stationary part of the grid. The variables are interpolated on the sliding boundary using the solution in the neighboring blocks.

In FINFLO, the solution is extended to the wall. An essential feature in the code is to separate flux calculation from the solution.

FINFLO computational approach includes also the use of the overlapping grid technique, that is, the so-called Chimera blocks can be added to grid. Morever, two-phase simulations are also possible. The cavitating flows can be simulated utilizing mass transfer rate model combined with the Volume-of-Fluid method.

GEOMETRY AND COMPUTATIONAL PARAMETERS

The geometry and non-dimensional flow parameters used in the computations are essentially same as those provided by Anderson et al. (1998) and Read et al. (2003) for the NACA0012-profile. The chord of the foil is 10 cm long.

The 2D grid is shown in Figure 1 together with the conditions enforced in the various boundaries. The EXTERNAL condition is either an INLET (uniform inflow) or OUTLET (zero gradient velocity-constant pressure) condition depending on the flow direction. The SLIDING boundary condition described in Sánchez-Caja et al. (1999) connects the rotating blocks to the stationary mesh.

The number of cells and the y^+ parameter are presented in Table 1. The coordinate system is shown in Figure 2.

The instantaneous angle of attack $\alpha(t)$ can be expressed approximately in terms of the inflow velocity U, foil pitch angle $\theta(t)$, and heave $h(t)$ with an angular frequency ω,

$$\tan(\alpha(t) - \theta(t)) = \frac{1}{U}\frac{dh}{dt}(t) \qquad (1)$$

The motion of the flapping foil can be described, for example, by the maximum angle of attack α_{max} and Strouhal number St. The maximum angle of attack can be approximated as follows

$$\alpha_{max} = \tan^{-1}\left(\frac{\omega h_0}{U}\right) - \theta_0 \qquad (2)$$

In the current simulations, the phase lag between the pitch and heave motions is set to 90 deg. The Strouhal number is expressed in terms of the frequency $f=\omega/(2\pi)$

$$St = \frac{2h_0 f}{U} \qquad (3)$$

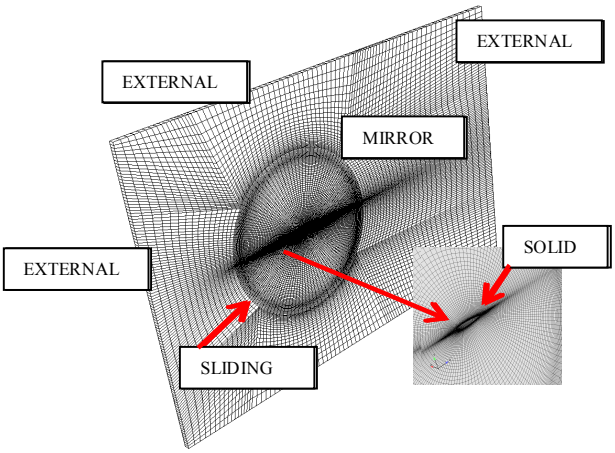

Figure 1: A schematic view of flapping foil the meshe together with the boundary conditions.

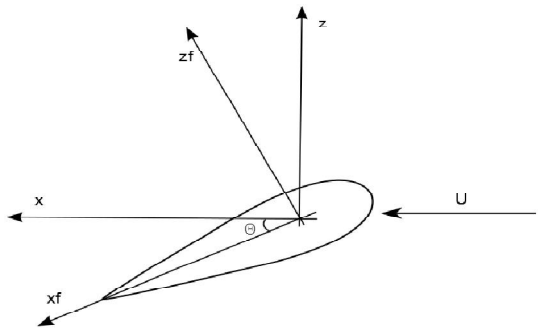

Figure 2: The coordinate system

Table 1: Grid figures

Number of cells	33024
y^+	~1

Table 2: Main parameters describing the computed cases

case	α_{max}	*St*
1	15.0	0.2
2	15.0	0.3
3	15.0	0.4
4	5.0	0.2
5	5.0	0.4
6	20.0	0.2
7	20.0	0.3
8	20.0	0.4
9	10.0 (5.0)	0.1
10	10.0	0.2
11	10.0	0.3
12	10.0	0.4
13	30.0	0.2
14	30.0	0.3
15	30.0	0.4
16	25.0	0.2
17	25.0	0.4
18	5.0	0.15
19	10.0	0.15
20	15.0	0.15
21	10.0	0.1

The computations were carried out at two Reynolds numbers, 40000 and 150000. The former corresponds to the experimental conditions in Anderson (1998) et al. and Read (2003) et al. with an inflow of 0.4 m/s. The latter is for an inflow velocity of 1.5 m/s. The main computational parameters are shown in Table 2. Case 9 was computed using α_{max}=5 deg for Re=40000 and α_{max}=10 deg for Re=150000.

VALIDATION OF PERFORMANCE PARAMETERS

The computed performance coefficients are compared with published experimental data. The average thrust force over one cycle can be determined as follows

$$\bar{F}_X = \frac{1}{T}\int_0^T F_x(t)dt \qquad (4)$$

The average hydrodynamic power over one cycle is determined analogously

$$\bar{P} = \frac{1}{T}\left(\int_0^T F_z(t)\dot{h}(t)dt + \int_0^T Q(t)\dot{\theta}(t)dt\right) \qquad (5)$$

where $Q(t)$ is the instantaneous torque and $F_z(t)$ is the instantaneous vertical force.

The thrust and power coefficients can be evaluated using expressions (4) and (5)

$$c_T = \frac{\bar{F}_X}{\frac{1}{2}\rho c V_0^2} \tag{6}$$

$$c_p = \frac{\bar{P}}{\frac{1}{2}\rho c V_0^3} \tag{7}$$

where ρ is the density and c the chord.

Finally, the efficiency of the flapping foil can be obtained as follows

$$\eta_O = \frac{c_T}{c_P} \tag{8}$$

The computed and experimental efficiencies are presented in Figures 3a-3c. The blue dots correspond to the computed cases and the isocurves are obtained by interpolation. The region of maximum computed efficiency is located at values of α_{max} somewhat smaller than experiments. The k-ω turbulence model estimates the high-efficiency region to be somewhat larger than experiments.

For Re=40000 the flow is expected to be mainly laminar. In principle, the computed efficiency compares reasonably well with the experimental efficiency if the differences in flow regime are taken into account in the comparison. In the computations, the maximum efficiency is obtained for lower maximum angles of attack (about 10 deg). The lower computed efficiency at 15 deg is most probably due to the higher friction in the fully turbulent computations relative to the tests where the flow is expected to be mostly laminar.

The computed thrust coefficients are larger than experimental ones for low maximum angles of attack (about 10 deg), and similar to measurements, for large angles of attack. The reason for this behavior can be related to the fact that for turbulent flow, separation is delayed for lower angles, and consequently, so is thrust breakdown. In other words, in turbulent regime the flow is more attached for low angles of attack, which results in efficiency improvement and larger thrust. At the higher Reynolds number Re=150000 the efficiency improves slightly. The shape of the contour remains similar, but the magnitude of efficiency increases throughout the (α_{max},St)-space.

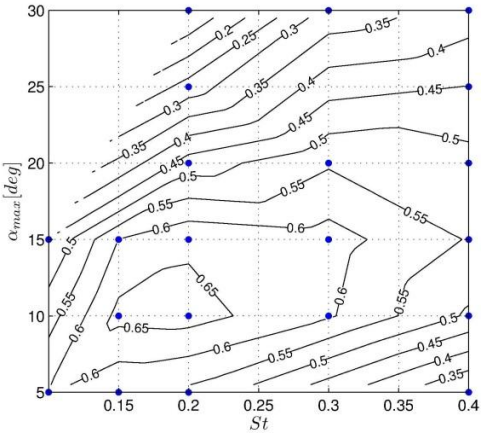

Figure 3a: Efficiency computed with the k-ω turbulence model as a function of α_{max} and St. (Re=40000)

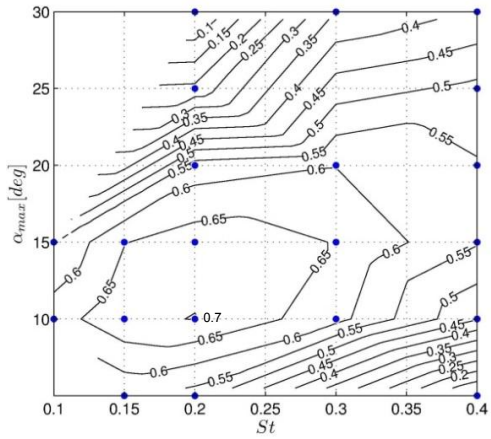

Figure 3b: Efficiency computed with the k-ω turbulence model as a function of α_{max} and St. (Re=150000)

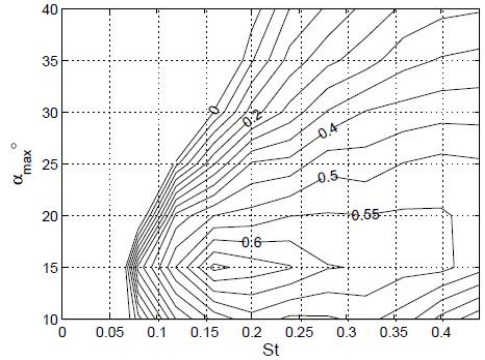

Figure 3c: The efficiency as a function of α_{max} and St, Read et al. (2003)

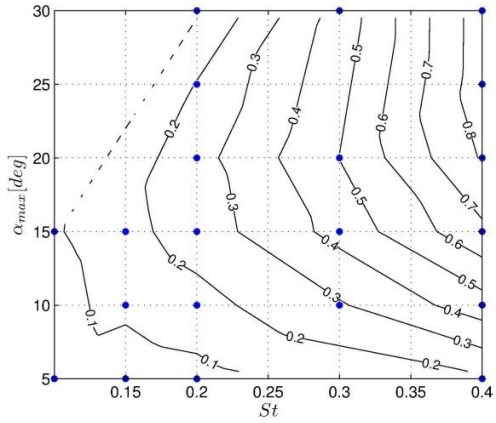

Figure 4a: Thrust coefficient computed with the k-ω turbulence model as a function of α_{max} and *St* Re=40000

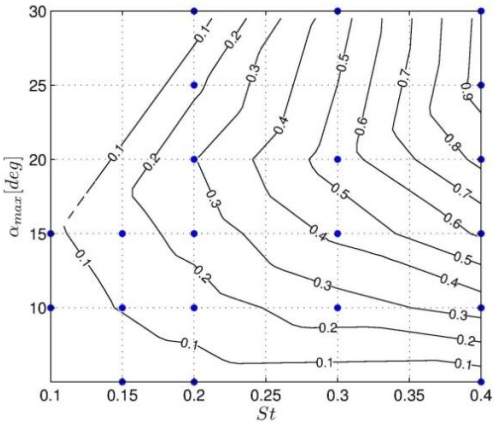

Figure 4b: Thrust coefficient computed with the k-ω turbulence model as a function of α_{max} and *St* Re=150000

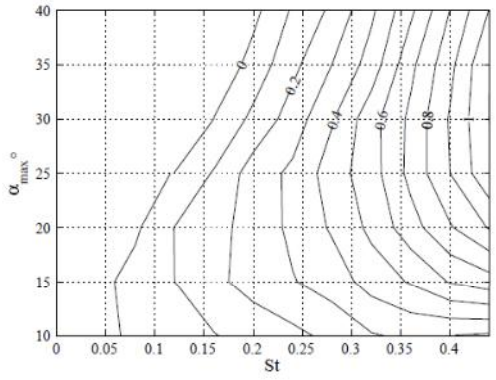

Figure 4c: Thrust coefficient as a function of α_{max} and *St*, Read et al. (2003)

The thrust coefficients are shown in Figures 4a-4c. Again, quantitative differences between the computed and experimental coefficients can be observed, but generally, the shape of the contours is similar. At the higher Reynolds number Re=150000 the thrust coefficient increases and the efficiency improves as shown in Figure 3b.

ANALYSIS OF ADDED MASS AND DAMPING

The analysis in frequency domain could be conducted using, for example, Fourier analysis. In this work, the first terms of Fourier series were fitted to the vertical force in order to determine the added mass and damping components. In principle, the coefficients include the memory effects due to the viscous contributions. Alternatively, a Morison-type fitting could be used, in which the velocity-dependent component is nonlinear, that is, the drag force term. In the present work, only the vertical translational motion is considered.

The analysis is carried out in two different coordinate systems: the inertial one and the one fixed to the body. In the inertial system the force decomposition leads to the following fit

$$F_z = m_{zz}\ddot{z} + c_{zz}\dot{z} \tag{9}$$

where F_z is the vertical force, m_{zz} is the added mass and c_{zz} is the damping. The state vector is defined by

$$(z, \dot{z}, \ddot{z}) = (z_0\cos(\omega t), -\dot{z}_0\sin(\omega t), -\ddot{z}_0\cos(\omega t)).$$

In the body reference system, the following fit is utilized

$$F_{zf} = m_{zzf}\ddot{z}_f + c_{zzf}\left(\dot{z}_f + U_{zf}\right) \tag{10}$$

where m_{zzf} and c_{zzf} are the added mass and damping terms in the body coordinate system, respectively, and F_{zf} is the instantaneous vertical force perpendicular to the foil.

In Equation (10) the acceleration component related to the added mass term is the vertical acceleration of the foil. On the other hand, the velocity imposed for the damping term is a combination of the vertical velocity $(\dot{z}_f)$ and the projection of the uniform flow on the local reference (U_{zf}). The uniform velocity is constant in time, and therefore does not contribute to the acceleration. Consequently, the instantaneous

acceleration in the coordinate system fixed to the body is evaluated as follows

$$\ddot{z}_f = \ddot{z}_0 \cos(\omega t)\cos(\theta) \quad (11)$$

Similarly, the vertical foil velocity can be expressed as

$$\dot{z}_f = \dot{z}_0 \sin(\omega t)\cos(\theta) \quad (12)$$

The contribution from the uniform flow is taken into account by the term

$$U_{zf} = U\sin(\theta) \quad (13)$$

The x-force in the body-fixed coordinates could also be derived and decomposed into added mass and damping terms in analogous way, but we restrict our analysis to the vertical component.

The non-dimensional added mass coefficient is defined as follows,

$$m'_{zz} = \frac{4 \cdot m_{zz}}{\pi \rho c^2};\ m'_{zzf} = \frac{4 \cdot m_{zzf}}{\pi \rho c^2} \quad (14)$$

whereas the damping coefficient for a 2D-foil can be evaluated by the following expression,

$$c'_{zz} = \frac{2 \cdot c_{zz}}{f \rho c^2};\ c'_{zzf} = \frac{2 \cdot c_{zzf}}{f \rho c^2} \quad (15)$$

In principle, the approach works for small values of pitching motions, θ_0. However, for large values, additional terms (pitch velocity and acceleration) should be added in equation (10). The 90 deg delayed pitch contribution cannot be isolated with the traditional fitting when coupled to heave, and therefore such additional terms will not be considered now.

RESULTS

The added mass coefficient m'_{zzf} and the damping coefficient c'_{zzf} are shown in Figures 5 and 6, respectively, as a function of the angle α_{max} and St for Re=40000. The added mass coefficient m'_{zz} in the inertial coordinate system is presented in Figure 7. The non-dimensional added mass coefficients as defined in (14) represent the ratio of computed added mass to the theoretical added mass of a flat plate according to potential flow theory. The coefficients m'_{zzf} and m'_{zz} include both potential and viscous flow contributions. The added mass and damping coefficients in the inertial coordinate system are presented in Figure 7 and 8, respectively, for Reynolds numbers 40000 and 150000.

The reference system of coordinates seems to have only minor impact on the added mass coefficient distributions. According the current simulations the inertial coordinate system could then be used to determine the added mass terms. For the damping terms as shown in Figures 6 and 8, the outcome is somewhat different, i.e. the damping coefficient c'_{zzf} was almost constant with respect to the Strouhal number.

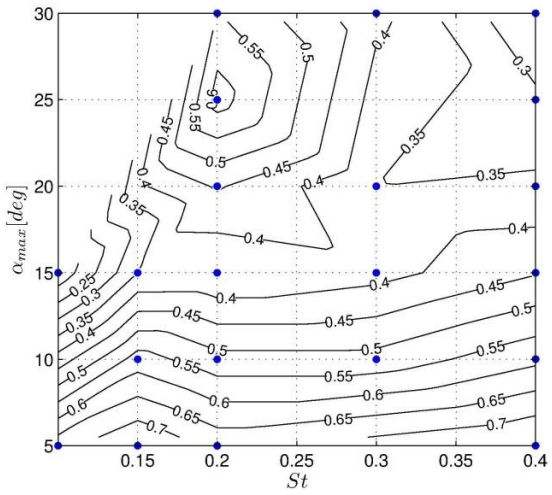

Figure 5: Added mass coefficient m'_{zzf} as a function of α_{max} and St, Re=40000

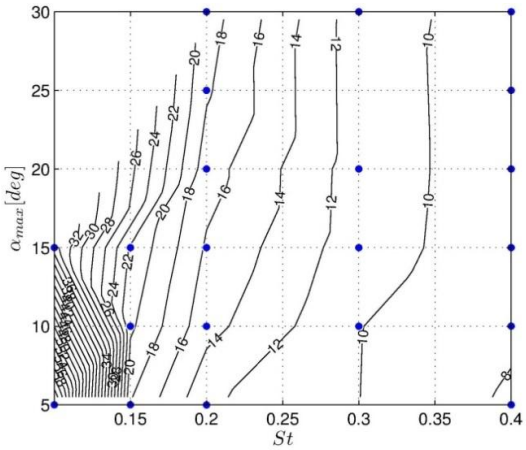

Figure 6: Damping coefficient c'_{zzf} as a function of α_{max} and St, Re=40000.

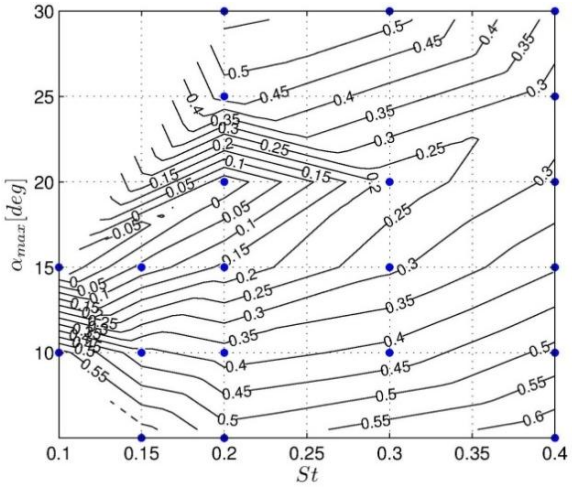

(a)

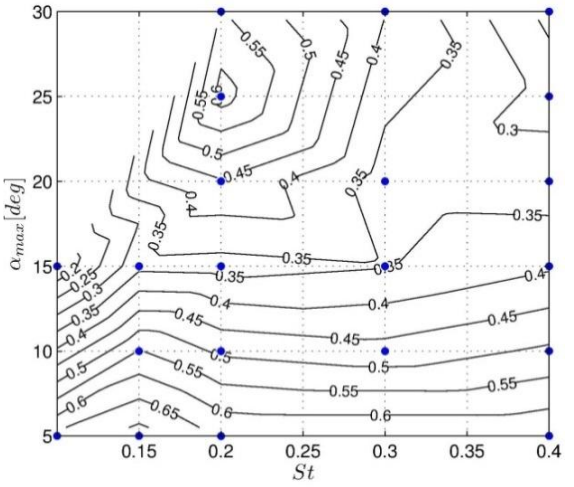

(b)

Figure 7: Added mass coefficient m'_{zz} as a function of α_{max} and St, top: Re=150000, bottom: Re=40000

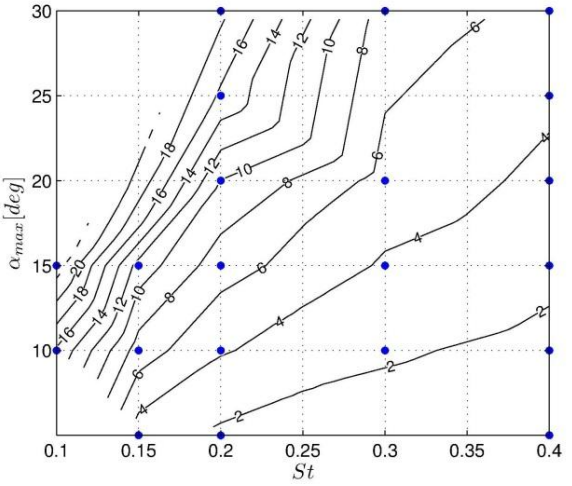

(a)

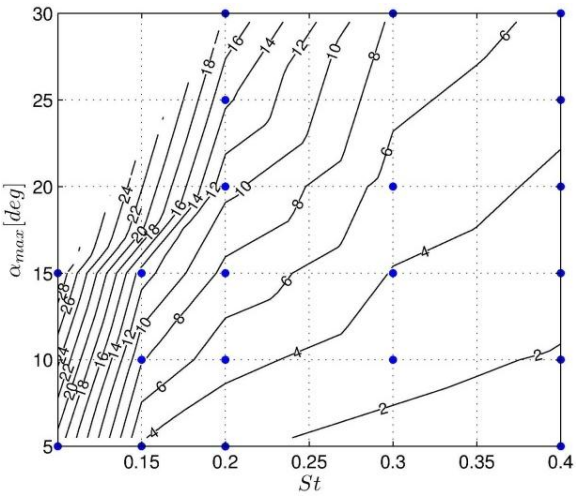

(b)

Figure 8: Damping coefficient c'_{zz} as a function of α_{max} and St, top: Re=150000, bottom: Re=40000

The Reynolds number has a significant effect on the added mass coeffcient m'_{zz}. Particularly at the (α_{max}=15-20 deg, St<0.2)-space the magnitude of m'_{zz} changes drastically. For example, for Case 6 with Re=150000 m'_{zz}=-0.01 whereas for Re=40000 m'_{zz}=0.45. For the damping coefficient, a similar behavior cannot be observed. According to Figure 8 the magnitude of c'_{zz} is quite similar for both Reynolds numbers.

Note also that the added mass coefficients are rather constant for the low maximum angles of attack (i.e. α_{max} =10 deg.). However, they change significantly for larger angles (α_{max} =20 deg).

An explanation for this behavior can be found by considering the Cases 6 and 10. The large pitching motions present in the former case contribute also to the total force, which has not been included in the harmonic fitting. However, the smaller pitch motions

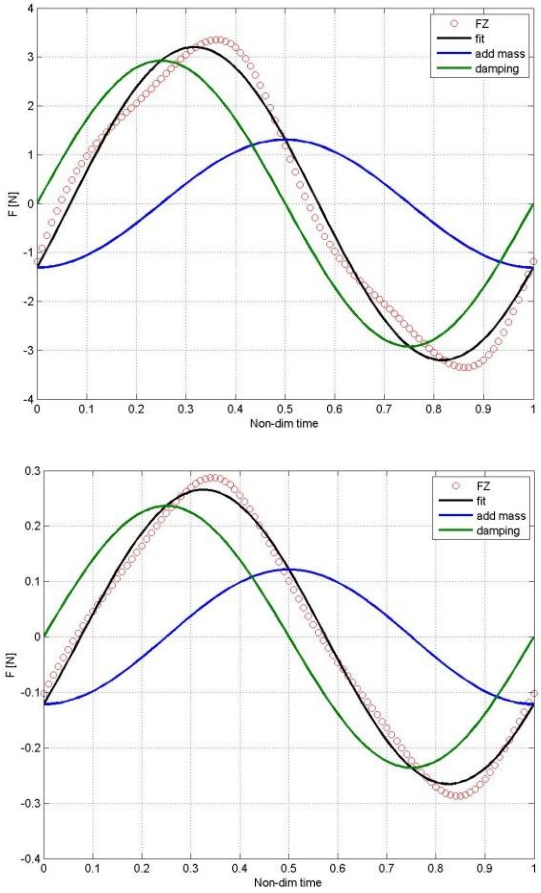

Figure 9: Time history of F_z together with the total force, added mass and damping term fittings, Case 10, top: Re=150000, bottom: Re=40000.

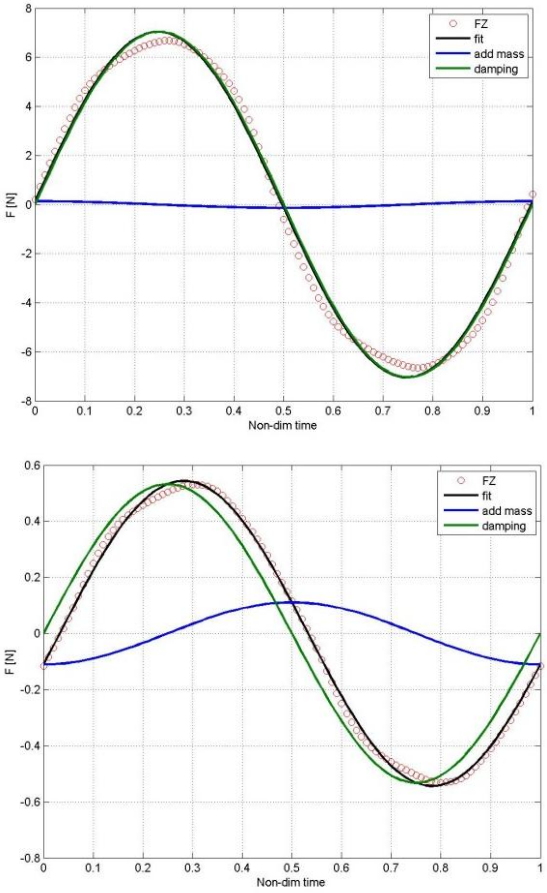

Figure 10: Time history of F_z together with the total force, added mass and damping term fittings, Case 6, top: Re=150000, bottom: Re=40000

in Case 10 do not contribute significantly to the total force and therefore, the fitting technique yields reasonable results.

The time histories of the vertical force for Cases 10 and 6 are examined more carefully in Figures 9 and 10. Case 10 with a theoretical angle of attack rather small (α_{max}=10 degrees) provides better efficiency than Case 6. The amplitude of the vertical force (Case 10) is rather small (about half) compared to Case 6 shown in Figure 10. The evaluated forces are almost linear. For Case 10 the ratio of fitted added mass and damping forces are similar for the two Reynolds numbers.

For Case 6, the flow field is examined more in detail in Figures 11a-11f. The velocity field in [m/s] around the foil is shown for the two Reynolds numbers.

According the URANS simulations leading edge separation occurs in the Case 6, which affects the phase shift and the sign of the added mass coefficient. At the time level 0.48 (Figure 11d) the structure of separation clearly changes with the Reynolds number. Leading edge separation is present at low Reynolds number, whereas at the Reynolds number 150000 the separation is confined downstream towards the trailing edge.

CONCLUSIONS

The flow around a flapping foil has been analyzed using an URANS method. Two flow conditions were evaluated corresponding to Reynolds numbers of 40000 and 150000. The efficiency and thrust

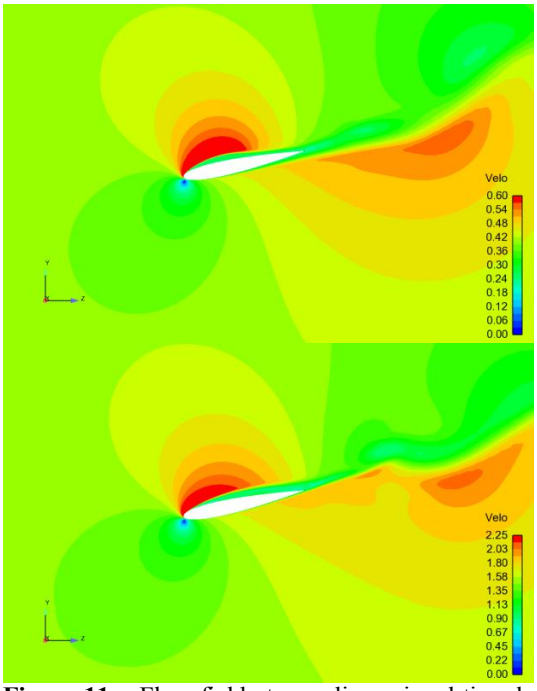

Figure 11a: Flow field at non-dimensional time level 0.24, top: Re=40000, bottom Re=150000

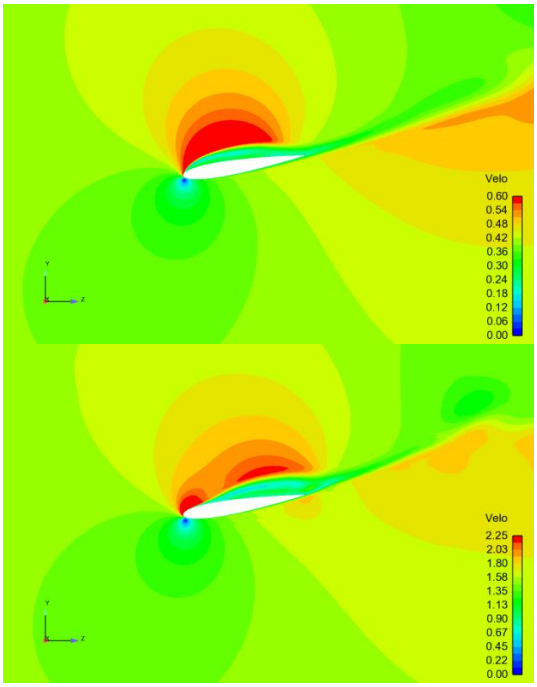

Figure 11b: Flow field at non-dimensional time level 0.36, top: Re=40000, bottom Re=150000

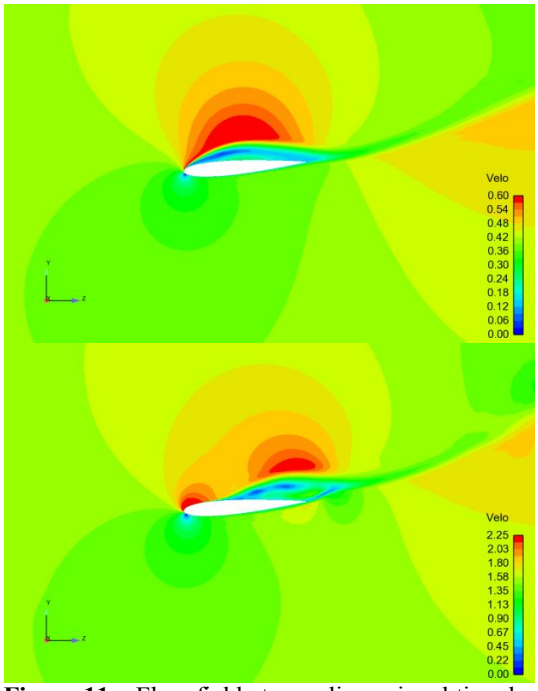

Figure 11c: Flow field at non-dimensional time level 0.44, top: Re=40000, bottom Re=150000

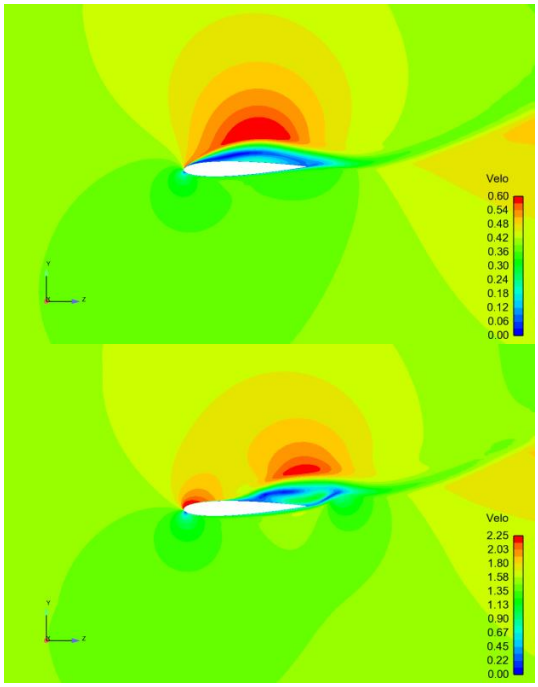

Figure 11d: Flow field at non-dimensional time level 0.48, top: Re=40000, bottom Re=150000

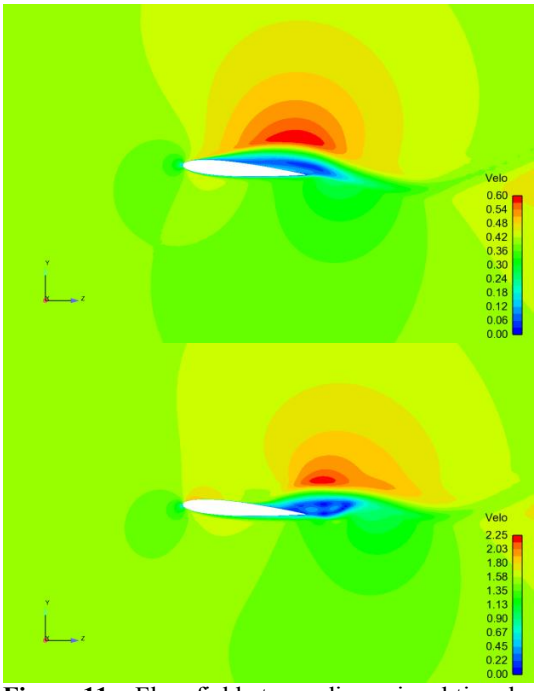

Figure 11e: Flow field at non-dimensional time level 0.56, top: Re=40000, bottom Re=150000

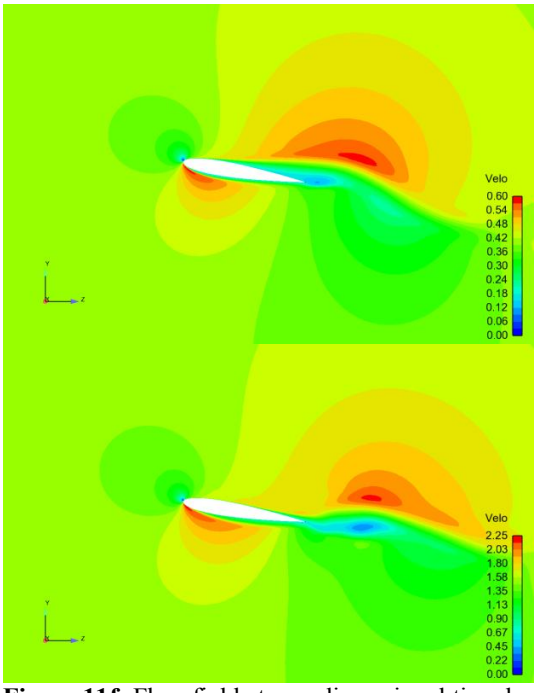

Figure 11f: Flow field at non-dimensional time level 0.64, top: Re=40000, bottom Re=150000

coefficients were computed as a function of (St, α_{max}), and compared with experimental results. The agreement was found to be reasonable when differences in flow regime are considered since the computations were performed for fully turbulent flow whereas the test are made in a mostly laminar environment. The computed high-efficiency region was located in slightly different space in (St, α_{max})-contour due to the decrease of separation in the computed turbulent flow relative to the mostly laminar flow of the tests.

In the literature, there is a seemingly disagreement about conditions of optimum performance for instantaneous angles of attack. Vermeiden et al. (2012) found optimum angles of attack around 10 deg. On the other hand, Reads et al. (2003) or Anderson et al. (1998) found the most efficient advance ratios at about 15-30 degrees.

In fact, the experiments made by Anderson et al. are at low Reynolds number (Re) of the order of 1100-40000 whereas those of Vermeiden et al. are at high Re close to half a million. At low Reynolds numbers viscous effects are important and it is very difficult to suppress leading edge separation. In such conditions, viscous-related drag can be decreased by reverse Karman vortex shedding. However, at high Reynolds numbers, viscous effects are not so important at low angles of attack and setting the foil with large angles near stall would mean increasing unnecessarily the production of viscous drag. The findings of Vermeiden et al. point to this direction. Therefore, it seems that the optimization of flapping foils for fully turbulent flows should be based on different grounds than that at low Reynolds numbers. Low angles of attack should be sought in optimum conditions at full scale.

The results of the present investigation seem to be in line with the findings of both Anderson et al. (1998) (or Reads et al. 2003) and Vermeiden et al. (2012). The former found higher efficiencies for large angles of attack for laminar flows and the latter around low angles around 10 deg for turbulent flows.

The added mass and damping coefficients of a flapping foil have been derived from first order harmonic fittings of the computed force components. Our focus was set to determine the vertical coefficients. They were also parameterized as a function of (St, α_{max}). The coefficients were determined in two coordinate systems, i.e. in the inertial and body-fixed coordinate ones for the lower Reynolds number cases. The choice of coordinate system does not have considerable influence to the

parametrization of the added mass coefficient – the contours given as a function of (St, α_{max}) were quite similar with both coordinate systems. However, the contours of constant damping coefficient were slightly different in (St, α_{max})-space, i.e. the damping coefficient was almost constant with respect to the Strouhal number.

The present approach for the analysis of added mass and damping terms is intended for small values of pitch motions. Large values would lead to unrealistic results. The reason is that 90 deg delayed pitch contribution cannot be isolated with the traditional fitting when coupled to the heave.

The flow fields at St=0.15 α_{max}=20° (Case 6) were studied in more detailed for the two Reynolds numbers. It was found that leading edge flow separation occurs at both Reynolds numbers. The separated flow seems to reduce the performance of the foil.

REFERENCES

Anderson, J. M., Streitlien, K., Barrett, D. S., Triantafyllou, M. S., 1998. Oscillating foils of high propulsive efficiency. Journal of Fluid Mechanics 360, 41–72

Ashraf , M. A., 2010. Numerical simulation of the flow over flapping airfoils in propulsion and power extraction regimes. Canberra, Australia, *The University of New South Wales at Australian Defence Force Academy*. Ph. D. Thesis.

Barannyk, O, Buckham, B. J., Oshkai, P. On performance of an oscillating plate under water propulsion system with variable chordwise flexibility at different depths of submergence. Journal of Fluids and Structures 28 (2012) 152–166.

Cebeci, T., Platzer, M., Chen, H., Chang, K.-C. Shao, J. P., 2004. Analysis of Low-Speed Unsteady Airfoil Flows. Horizons Publishing Inc.

Hover F, Haugsdal Ø, Triantafyllou M. Effect of angle of attack profiles in flapping foil propulsion. J Fluids Struct 2004; 19:37–47.

Isogai, K., Shinmoto, Y., Watanabe, Y., 1999. Effects of dynamic stall on propulsive efficiency and thrust of flapping airfoil. AIAA Journal 37 (10), 1145–1151.

Miettinen, A., and T. Siikonen. Application of pressure- and density-based methods for different flow speeds. International Journal for Numerical Methods in Fluids (2015).

Read, D. A., Hover, F. S., Triantafyllou, M. S., 2003. Forces on oscillating foils for propulsion and maneuvering. Journal of Fluids and Structures 17 (1), 163–183.

Sánchez-Caja, A. & Martio, J. On the optimum performance of oscillating foil propulsors J Mar Sci Technol (2016). doi:10.1007/s00773-016-0397-7

Sánchez-Caja, A., Sipilä, T., Pylkkänen, J. Simulation of the Incompressible Viscous Flow around an Endplate Propeller Using a RANSE Solver, 26th Symposium on Naval Hydrodynamics Rome, Italy, 17-22, 2006.

Sánchez-Caja, A., Rautaheimo, P., Salminen, E., and Siikonen, T. Computation of the Incompressible Viscous Flow around a Tractor Thruster Using a Sliding Mesh Technique, 7th International Conference in Numerical Ship Hydrodynamics, Nantes (France), 1999.

Vermeiden J. G., Kooiker, K., Lafeber, F.H. van Terwisga, T., Cerup-Simonsen B., Folsø R. A Systematic Experimental Study on Powering Performance of Flapping Foil Propulsors. 29th Symposium on Naval Hydrodynamics, Gothenburg, Sweden, 26-31 August 2012.

Young, J., Lai, J. C. S., 2004. Oscillation frequency and amplitude effects on the wake of plunging airfoil. AIAA Journal 42 (10), 2042–2052

DISCUSSION

Sverre Steen, Department of Marine Technology NTNU, (Norway).

Thank you for sharing these interesting results.

I could not find information about heave amplitudes – the effective angle of attach will be a function of both heave and pitch amplitude, and the heave amplitude seems not to be given. What heave amplitudes were applied? What is your opinion on the importance of the heave amplitude?

You argue that the simple single-harmonic motion pattern with 90 degrees phase difference between heave and pitch is the best, since it produces the most regular reverse Von Karman vortex street. Did you try other motion patterns or phase angles? Also, did you study the resulting Von Karman vortex street?

I understand that the focus of the paper is mostly on the methodology of computation. However, I would still like your comments on the practical implications of the results and your view on the attractiveness of the flapping foil as propulsion device. Do you think the resulting efficiencies are sufficient to convince equipment supplier and ship owners to change from propellers to flapping foils? And, what do you recommend to be done in order to make the flapping foil attractive for practical use?

AUTHORS' REPLY

The ratio of heave amplitude to chord is that of Read et al. (2003) experiments. i.e. $h_0/c=0.75$ (now included in the main text). We think that such ratio is one of the key parameters in foil optimization. In fact, Vermeiden el al. (2012) have shown in tests at Re= 400,000 that flapping foils are optimal for low chord-heave ratios (high h_0/c) operating at high transverse acceleration for maximum angles of attack of 10-11 deg. They tried to increase the chord-heave ratio in an attempt to reduce accelerations, but they found an unexpected result: the strong decrease of efficiency with growing chord-heave ratios, which could not be explained by considerations on aspect ratio, reduced frequency or viscous losses. This topic has been analyzed in detail in Sanchez-Caja & Martio, (2016), where added mass effects were identified as responsible for such behavior.

We have set 90 deg phase difference in our computations since this value is the one used in the experiments, and the optimum phase lag should be close to it. Concerning the reverse vortex street, there is an opinion that high efficiency is associated with dynamic stall and leading edge vorticity formation, along with properly timed kinematics to deposit this vorticity on the `correct side' of the wake. However, this statement should be formulated in our opinion somewhat differently. We think that, generally speaking, leading edge vorticity is harmful since it means viscous losses, and additionally contributes to the distortion of the reverse vortex street generated at the trailing edge by the foil propulsive motion. It is true that when leading edge separation cannot be avoided the timing of the vorticity deposition should be carefully adjusted in order not to have the reverse Karman street spoiled, but it would be better to avoid leading edge separation as much as possible. Moreover, it would be very difficult to reach in practical applications the right timing of leading edge vortex shedding due to the flow fluctuations present in the highly unsteady turbulent wake of the ship.

In our opinion, many efforts to improve the performance of propulsion concepts based on oscillating foils have gone in a wrong direction since research has been focused mainly on low Reynolds number studies while the area of interest for more relevant marine applications seems to be high Reynolds number. We think that this is one of the reasons why in the last decades much has been written about the high efficiency potential of flapping foil propulsion devices, but actual applications have been scarce.

Reynolds number effects have also contributed to a seemingly disagreement on optimum performance parameters. For example, optimum maximum angles of attack of 20-30 deg were reported by Anderson et al. (1998), versus 10-11 deg by Vermeiden el al. (2012). The former experiments were made at Re=1,100-40,000 (laminar flow) whereas the latter at Re=400,000. Most probably, phenomena like leading edge separation was not as relevant for the latter case as it was for the former one. Read et al. (2002) reports optimum angles around 15 deg for Re=40,000. He shows that as h_0/c grows, there is a tendency for maximum efficiency contours to shift to lower angles of attack. However, the level of 10 deg cannot be reached for the maximum contours as in our high Re computations, most probably due to laminar flow effects. In summary, it seems that optimization at low scales should be based on different grounds than that at large scales, and that large scales have more potential for efficiency gains.

Additionally, the neglect of added mass effects in design theories has resulted in large differences between predictions and experiments (Sanchez-Caja & Martio, 2016).

Answering now to your last questions, the other reason for having few applications is that the propulsive efficiency consists not only of hydrodynamic efficiency, but also of mechanical efficiency. The mechanism for flapping foil propulsion should be such that does not obscure the gains obtained in hydrodynamic efficiency. Ship owners and equipment suppliers will be interested in flapping foil propulsion when they see prototypes built with both hydrodynamic and mechanical solutions that clearly outperform current propulsion devices.

DISCUSSION

Vermeiden, J.G. Huygens Engineers BV, (Netherlands).

This work first links experimental measurements on flapping foils at laminar flow @ Re=40.000, with a harmonic pitching cycle resulting in a non harmonic cycle of angle of attack to computations at two different Reynolds number using advanced 2D computational RANS methods where the nominal angle of attack in both cases is identical. Acceptable differences between simulation and measurements are analyzed and justified in terms of predictable deviations resulting from simplifications inherent to the method.

This first part of the work provides valuable illustration of the hydrodynamic mechanisms that lead to high flapping foil efficiency at low Reynolds numbers and at high Reynolds numbers.

The differences of efficiency obtained through computation in the range of Reynolds numbers seem still to end up somewhat lower than e.g. the differences of efficiency in flight seen in nature with varying scale.

The second part of the work breaks down the computational result in two harmonic components: the damping component, in phase with motion, and the added mass component, with 90 degrees delay, which are fitted to the simulated data to add up to the fundamental. Two cases are then compared (10 and then 20 degrees of attack nominal) at both Reynolds numbers. The damping term scales linearly with angle of attack, but the added mass stays constant at high Reynolds and on the other hand vanishes at low Reynolds. This illustrates how leading edge separation occurs at low Reynolds. This type of analysis could possibly be carried further and explain the large effect of varying chord-length better. If presented the opportunity, the current commentator would also look at the ratio chord-length to minimum path curvature as a predictive indicator to efficiency losses because losses seem to concentrate at the position maxima of the fins.

AUTHORS' REPLY

Thanks for your comments. As you mention, we found that leading edge separation has a strong influence in added mass terms. We can consider added mass to consist of two components, one of potential nature and the other from viscous nature. In a previous paper (Sanchez-Caja & Martio, 2016), we have shown that the former component may have a strong influence in efficiency when the chord length is increased. Moreover, in the paper discussed here, the viscous component is shown to have also a significant impact on performance for large maximum angles of attack.

We have already commented in the reply to Prof. Steen about the effects of varying the chord length on efficiency. We agree that ratio of chord-length to path curvature may be used as predictive indicator to efficiency losses. In fact, the path curvature grows as the heave-chord ratio grows; they are similar indicators, being your proposal a more sophisticated indicator.